

## Chapter 6 Electron identification in MINOS

Chapter 4 showed how it is possible to measure the mixing parameters in a two-generation framework by identifying  $\nu_\mu$  CC events and measuring the  $\nu_\mu$  disappearance probability,  $P_{\mu\mu}$ . If it is also possible to identify  $\nu_e$  CC or  $\nu_\tau$  CC events then an independent and complementary analysis is possible. This describes a simple method to identify  $\nu_e$  CC events and fit the energy distribution of electron-like events to measure the neutrino mixing parameters. The identification of  $\nu_\tau$  CC events is more difficult and is studied in Chapter 8.

### 6.1 Electron identification

Several algorithms exist to identify  $\nu_e$  CC events in MINOS [72][85]. The algorithms typically search for events that are short compared to  $\nu_\mu$  CC events, are more compact than NC events and reach shower maximum earlier than hadronic events. A  $\nu_e$  CC efficiency of  $\sim 15\%$  with less than 1% background of  $\nu_\mu$  events has been obtained by using sophisticated pattern recognition algorithms on simulated MINOS data.

The electron identification algorithm described in this chapter uses simple cuts to produce a  $\nu_e$  CC efficiency and a  $\nu_\mu$  background inefficiency that is comparable to the simple procedure outlined in the MINOS proposal [69] ( $\nu_e$  CC efficiency = 27% and  $\nu_\mu$  background efficiency = 1%). Since the purpose of this section is to investigate  $\nu_\mu \rightarrow \nu_e$  oscillations with large  $\sin^2 2\theta$ , it is not necessary to achieve better than 1% background suppression here.

Figure 6.1 shows the discriminating variables used in this analysis. The top three plots are for  $\nu_e$  CC events and the bottom three plots are for NC events. The two left-hand plots show the summed pulse height in the first 10 planes (approximately 12 radiation lengths) divided by the total pulse height. Electromagnetic showers develop earlier than their hadronic counterparts and so the fraction of total pulse height deposited in the first 10 planes is larger. The centre plots show the RMS width (in centimeters) of events, calculated with respect to the  $z$ - axis. Electron showers tend to be somewhat narrower than hadronic showers. The two right-hand plots show distributions of total pulse height. Neutral current events have large missing energy and usually have smaller values of total pulse height than  $\nu_e$  CC events. A harsh cut on total pulse height, however, would affect the sensitivity of electron identification to neutrino oscillations with low  $\Delta m^2$ , since pulse height is directly

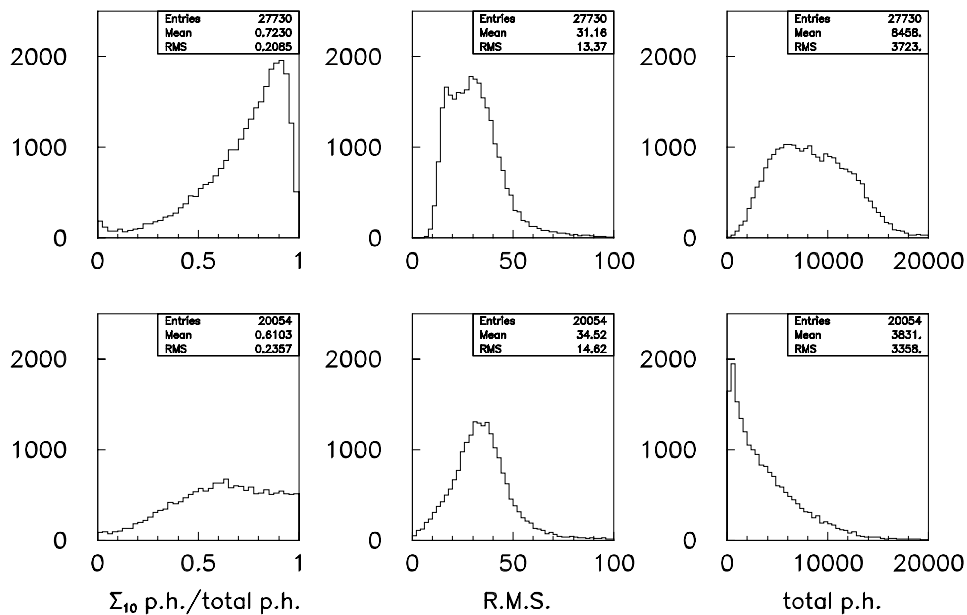


Figure 6.1 – The discriminating variables that are used for electron identification. The top plots are for  $\nu_e$  CC events and the bottom plots are for NC events. The variables are defined in the text.

related to neutrino energy.

Electron-like events in this analysis are defined by the following cuts:

- event length < 44 planes;
- pulse height in first 10 planes/total pulse height > 0.8;
- RMS < 20 cm;
- total pulse height > 1500 photoelectrons (this corresponds to approximately 3 GeV of visible energy. It has a very small effect on the  $\nu_e$  CC acceptance since the previous cuts favour  $\nu_e$  CC events with large visible energy).

Figure 6.2 shows the  $\nu_e$  CC efficiency and NC inefficiency plotted as a function of

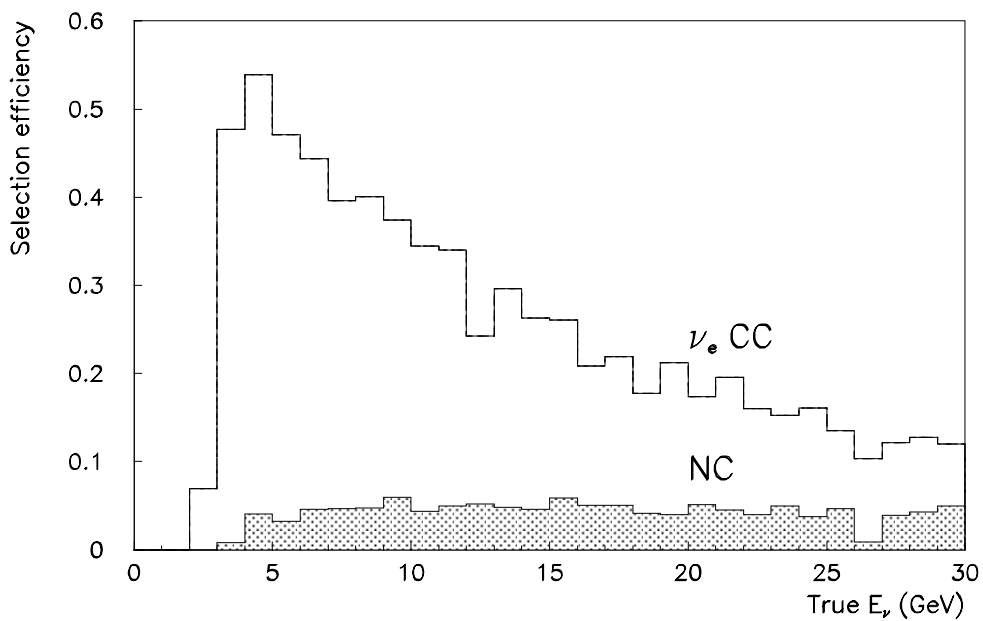


Figure 6.2 -  $\nu_e$  CC selection efficiency (open histogram) and NC inefficiency (shaded histogram) as a function of true neutrino energy.

true neutrino energy. The average  $\nu_e$  CC efficiency is 26% and the NC inefficiency is 4%. This background rate can be understood in the following way: the major background to  $\nu_e$  CC events is inelastic NC events where most of the energy goes into creating a single  $\pi^0$ . Assuming 33% of NC events have a large  $\pi^0$  fraction, these events have  $y > 0.5$  and the selection efficiency is 26%, then the expected background is  $0.33 \times 0.5 \times 0.26 = 4.3\%$  which is consistent with the Monte Carlo result.

The  $\nu_e$  CC selection efficiency is a strong function of neutrino energy. It is zero below 2 GeV and rises sharply to a maximum of  $\sim 50\%$  at 5 GeV. The efficiency then falls towards a value of 15% at 30 GeV. The reason for this is that electromagnetic showers become longer as the neutrino energy increases. As a consequence a smaller fraction of the total pulse height is contained in the first 10 planes. At very high energy, the showers become longer than 44 planes and therefore fail the event length cut.

The total pulse height is a good measure of electron neutrino energies. The left-hand plot of Figure 6.3 shows reconstructed neutrino energy (solid line), which is defined as total

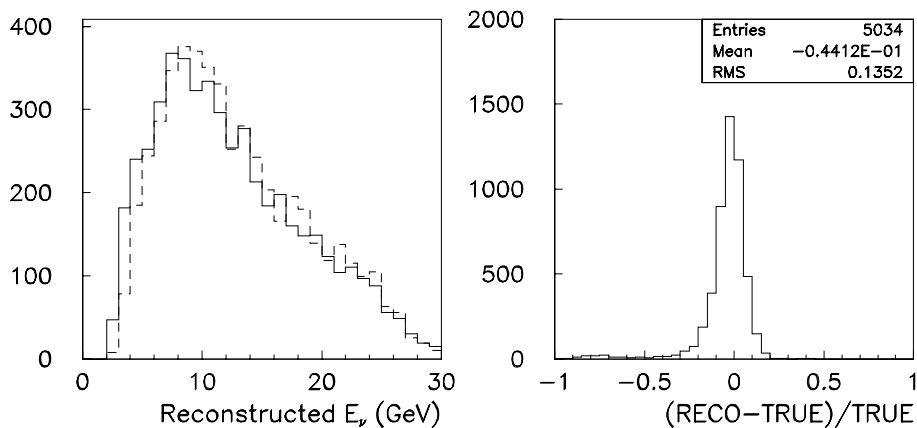


Figure 6.3 – Left-hand plot: reconstructed neutrino energy (solid histogram) and true neutrino energy (dashed histogram) for electron-like events. Right-hand plot: fractional error in energy measurement for these events.

pulse height/540, and true neutrino energy (dashed line) for electron-like events. There is good agreement between the two histograms. The right hand plot shows the fractional difference between reconstructed and true energies. This distribution has a *rms* of 13%, which, given a mean neutrino energy of 10 GeV, roughly corresponds to an energy resolution of  $\Delta E_\nu / E_\nu \sim 40\% / \sqrt{E_\nu}$ .

## 6.2 $\nu_e$ CC energy test in MINOS

If  $\nu_\mu \rightarrow \nu_e$  oscillations occur with large  $\sin^2 2\theta$  then it is possible to identify electron-like events using the cuts described above and to fit the resulting energy distribution in order to obtain a complementary (and independent) measurement of the mixing parameters to the  $\nu_\mu$  CC energy analysis described in Chapter 4.

The fitting procedure is similar to that described in section 4.5.1. Two Monte Carlo samples of  $\nu_e$  events are generated. The electron identification cuts are applied to the samples. The large 9.63 kiloton year exposure MCNO sample contains 3651 electron-like events and the 3.3 kiloton year exposure MCEXP sample contains 1383 events. Two-generation  $\nu_\mu \rightarrow \nu_e$  oscillations with mixing parameters  $\sin^2 2\theta$  and  $\Delta m^2$  are assumed. The weight  $W = \sin^2 2\theta \sin^2(1.27\Delta m^2 L / E_\nu)$  is calculated for each event and the event is accepted into the MCEXP sample if the random number  $R$  is less than  $W$ , where  $0 < R < 1$ . The 0.5%  $\nu_e + \bar{\nu}_e$  component of the beam is ignored since it has a negligible effect for oscillations with large  $\sin^2 2\theta$ .

Figure 6.4 shows the number of electron-like events expected in a 3.3 kiloton exposure of MINOS as a function of  $\Delta m^2$ , assuming  $\nu_\mu \rightarrow \nu_e$  oscillations with  $\sin^2 2\theta = 1$ . The contributions from  $\nu_e$  CC events that are due to  $\nu_\mu \rightarrow \nu_e$  oscillations, neutral current

events and the intrinsic  $\nu_e + \bar{\nu}_e$  beam component are shown separately. The number of electron-like events from  $\nu_\mu \rightarrow \nu_e$  oscillations is at least a factor of 10 (or more) larger than the background from NC and beam  $\nu_e + \bar{\nu}_e$  events. The expected number of electron-like events that are due to neutral current interactions (39 events for a 3.3 kiloton year exposure) is independent of the neutrino oscillation parameters. The number of electron events from interactions of beam  $\nu_e + \bar{\nu}_e$  is actually expected to *decrease* as a function of  $\Delta m^2$ , because they are depleted by  $\nu_e \rightarrow \nu_\mu$  oscillations so the 10 events predicted in Figure 6.4 is therefore an upper limit.

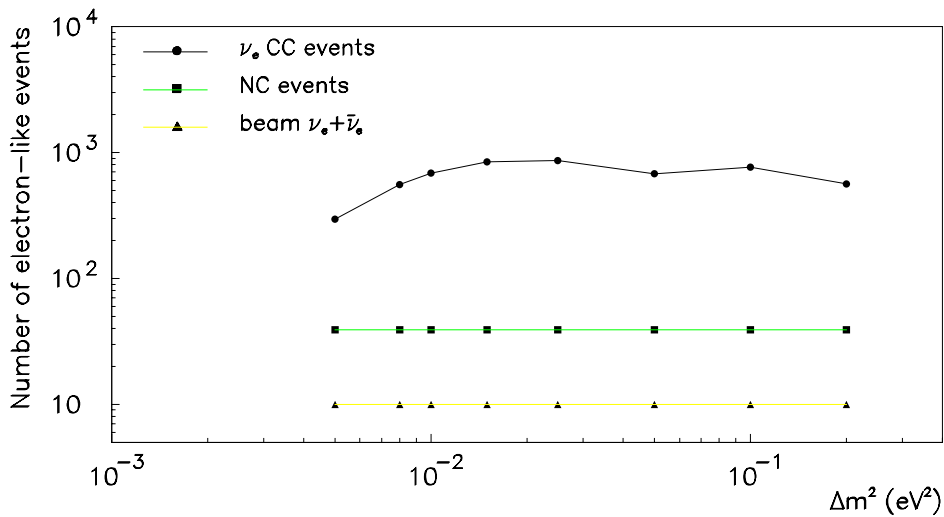


Figure 6.4 – The numbers of events that are classified as electron-like by the cuts described in this chapter, plotted as a function of  $\Delta m^2$ . Neutrino oscillations in the mode  $\nu_\mu \rightarrow \nu_e$  with  $\sin^2 2\theta = 1$  are assumed. The contributions from  $\nu_e$  CC events that are the result of  $\nu_\mu \rightarrow \nu_e$  oscillations, neutral current events and events due to the intrinsic  $\nu_e + \bar{\nu}_e$  component of the beam are shown separately.

Due to the small number of events in the MCEXP sample, the number of bins of  $E_{reco}$  used in the fit is reduced from 60 to 30. Poisson probabilities, rather than Gaussian probabilities, are assumed for the same reason:

$$P(m(i), n(i)) = \frac{1}{m(i)!} \times n(i)^{m(i)} \times e^{-n(i)}, \quad (6.1)$$

where  $m(i)$  and  $n(i)$  are the numbers of events in bin  $i$  of the MCEXP and MCNO  $E_{reco}$  distributions respectively and  $P(m(i), n(i))$  is the Poisson probability of observing  $m(i)$  events when  $n(i)$  are expected.

The log likelihood, neglecting terms in  $m(i)!$ , is:

$$\ln L = \sum_{i=1}^n (m(i) \times \ln n(i, \Delta m^2, \sin^2 2\theta) - n(i, \Delta m^2, \sin^2 2\theta)). \quad (6.2)$$

Note that this is the log likelihood and not the log likelihood ratio, that was used in Chapter 4.

Figure 6.5 shows a fit to a MCEXP sample with  $\Delta m^2 = 0.01 \text{ eV}^2$  and  $\sin^2 2\theta = 0.7$ , assuming  $\nu_\mu \rightarrow \nu_e$  oscillations. The left-hand plot shows a comparison between the error contours in neutrino mixing parameter space obtained from this fit to those obtained from the independent  $\nu_\mu$  disappearance fit described in Chapter 4. The thick line denotes the 68% confidence level contours for  $\nu_e$  appearance and the thin line is for  $\nu_\mu$  disappearance. The star indicates the true parameters. The right-hand plot shows the distributions of reconstructed electron neutrino energy for the MCEXP sample (error bars) and the best-fit MCNO sample (histogram). The agreement between the two distributions is very good ( $\chi^2 = 17 / 28$ ).

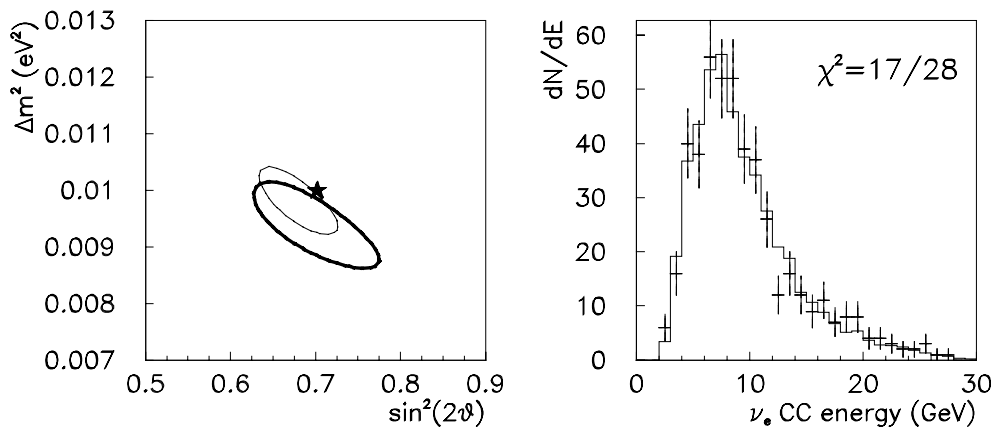


Figure 6.5 -  $\nu_e$  CC energy test for  $\Delta m^2 = 0.01 \text{ eV}^2$  and  $\sin^2 2\theta = 0.7$  and  $\nu_\mu \rightarrow \nu_e$  oscillations, assuming fixed normalisation. Left-hand plot: 68% C.L. error contours in neutrino oscillation parameter space. The thick line is for  $\nu_e$  appearance and the thin line is for  $\nu_\mu$  disappearance.

The star represents the true mixing solution. Right-hand plot: reconstructed neutrino energy distributions for the MCEXP sample (error bars) and the best-fit MCNO sample (histogram). A 3.3 kiloton year exposure of MINOS is assumed.

The contours are obviously larger for electron appearance since the  $\nu_e$  CC selection efficiency (26%) is much smaller than the efficiency for selecting  $\nu_\mu$  CC events (91%). Both fits are consistent with the true parameters and so electron appearance can act as an important cross-check of any result observed with  $\nu_\mu$  disappearance.

Figure 6.6 shows the results of fits to MCEXP samples with several values of  $\Delta m^2$  and  $\sin^2 2\theta = 0.7$ . In all four cases, the values of the parameters obtained by  $\nu_e$  appearance and  $\nu_\mu$  disappearance are consistent with each other and with the true parameters. Both fits produce large errors on the parameters at  $\Delta m^2 = 0.005 \text{ eV}^2$  since there is little neutrino flux below  $\sim 3 \text{ GeV}$ . The  $\nu_e$  appearance fit produces large errors at  $\Delta m^2 = 0.008 \text{ eV}^2$ , at which point the  $\nu_\mu$  disappearance can measure the parameters to  $\pm 10\%$ . This is due to the reduced selection efficiency and hence statistics for electron appearance at low neutrino energy.

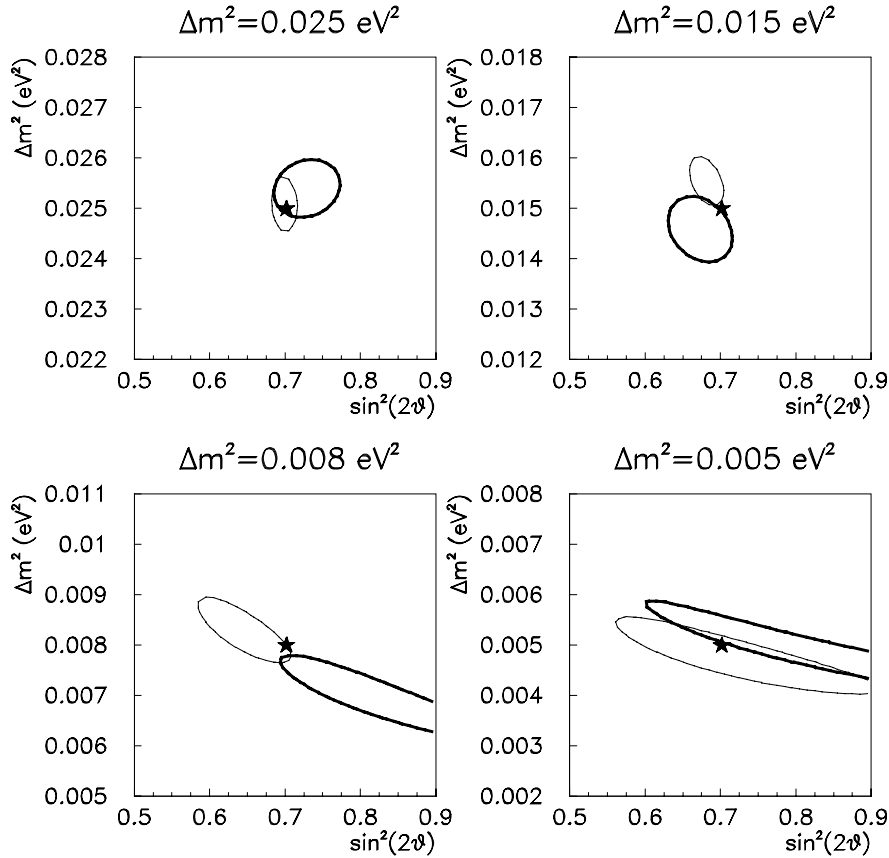


Figure 6.6 – Fits to MCEXP samples with various values of  $\Delta m^2$  and  $\sin^2 2\theta = 0.7$ , assuming  $\nu_\mu \rightarrow \nu_e$  oscillations and fixed normalisation. The 68% C.L. error contours are drawn. The thick lines are for  $\nu_e$  appearance fits and the thin lines are for  $\nu_\mu$  disappearance. A 3.3 kiloton year exposure of MINOS is assumed.

Figure 6.7 shows how the errors on the mixing parameters from a fit to the  $\nu_e$  CC energy distribution compare to those from the fits to the  $\nu_\mu$  CC energy distribution in Chapter 4. The fits assume that the normalisation is perfectly known. The top plot of Figure 6.7 shows that the errors on  $\Delta m^2$  from the two methods are comparable. The error on

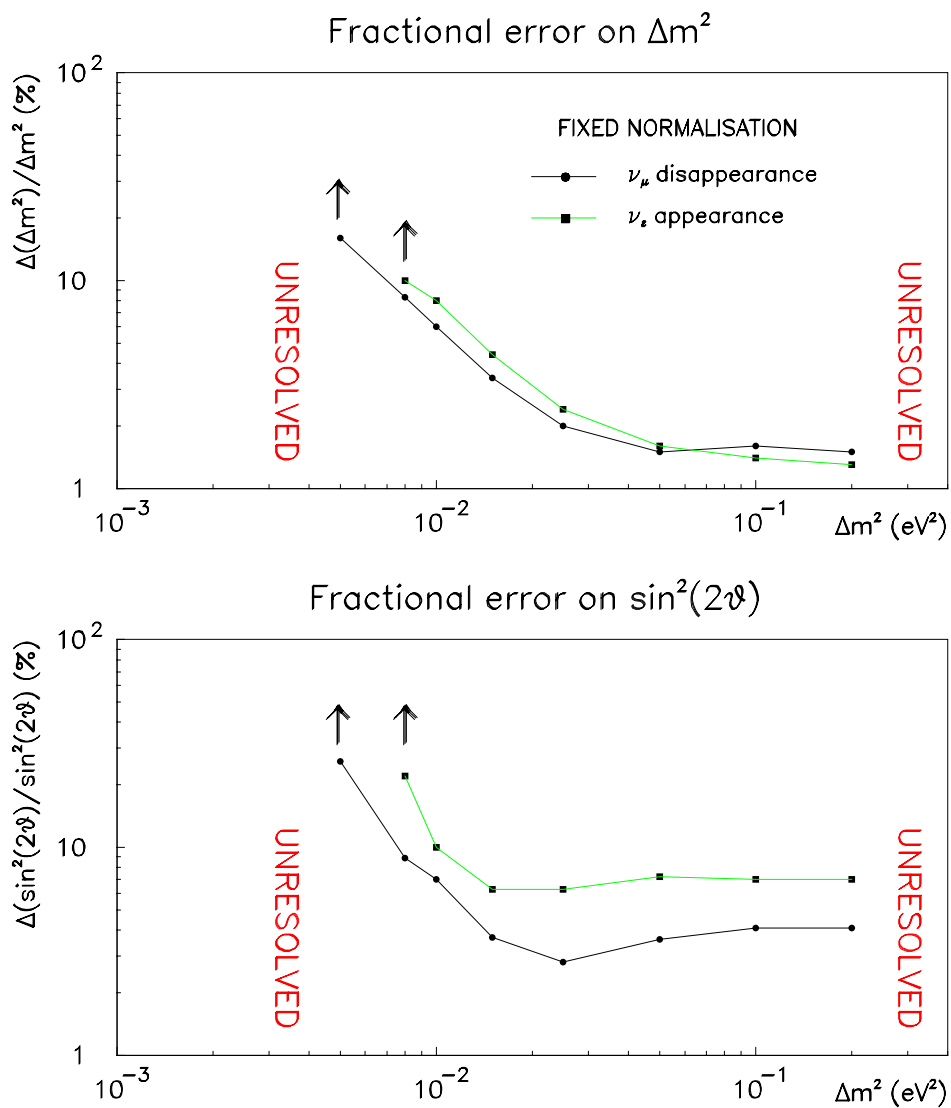


Figure 6.7 – Summary of parameter measurement errors for fits to neutrino oscillations with  $\sin^2 2\theta = 0.7$  and various values of  $\Delta m^2$ . The results of independent, fixed normalisation fits to  $\nu_\mu$  CC and  $\nu_e$  CC energy distributions are compared.

$\sin^2 2\theta$  is typically a factor of two larger for the electron appearance fits. This can be explained by the reduction in statistics for the electron appearance fits compared to the muon disappearance fits. The factor of four difference in the selection efficiencies should result in error contours for electron appearance fits that are twice as large as their muon appearance counterparts. This is what is observed.

If a shape-only fit is performed on any of the  $\nu_e$  CC energy distributions considered above then it is impossible to extract a value of  $\sin^2 2\theta$ . This is because the shape of an appearance signal only depends on  $\Delta m^2$ , whereas the shape of a disappearance signal (a dip in the  $\nu_\mu$  CC energy distribution) depends both on  $\Delta m^2$  and  $\sin^2 2\theta$ . The normalisation information is therefore crucial to extract a measurement of neutrino oscillation parameters from an appearance signal.

Figure 6.8 summarises the errors on  $\Delta m^2$  obtained by independent shape-only fits to muon disappearance and electron appearance signals. The plot shows that the errors on  $\Delta m^2$  are comparable.

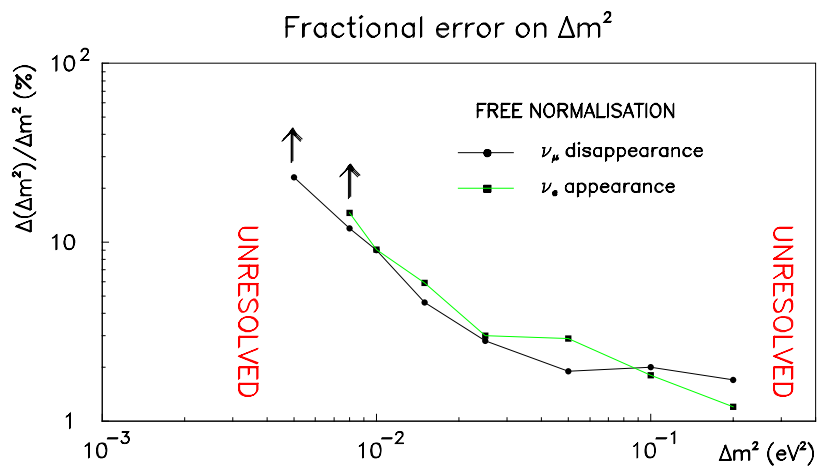


Figure 6.8 – Comparison of errors on  $\Delta m^2$  from independent, shape-only fits to  $\nu_\mu$  disappearance and  $\nu_e$  appearance signals.

### 6.3 Conclusions

This chapter has shown that it is possible to use the energy distribution of electron-like events (mostly  $\nu_e$  CC interactions) to obtain an independent and complementary measurement of the neutrino mixing parameters to the  $\nu_\mu$  CC analysis described in Chapter 4 if oscillations occur with large  $\sin^2 2\theta$ . The simple cuts described above select  $\nu_e$  CC events with 26% efficiency and the background from neutral current and the intrinsic  $\nu_e + \bar{\nu}_e$  component of the beam is at least a factor of 10 smaller than the  $\nu_\mu \rightarrow \nu_e$  signal if oscillations occur in this mode with  $\sin^2 2\theta \sim 1$ .

The errors on the mixing parameters obtained from fits to  $\nu_e$  energy distributions are larger than the corresponding errors from  $\nu_\mu$  disappearance fits because the selection efficiency is a factor of four smaller. This results in errors on  $\sin^2 2\theta$  that are larger by a factor of two, assuming the rate normalisation is perfectly known. If the normalisation is not known at all then it is impossible to measure  $\sin^2 2\theta$  from  $\nu_e$  appearance because the shape of the  $\nu_e$  CC energy distribution is independent of  $\sin^2 2\theta$ .

If a large effect is observed in the  $\nu_\mu$  disappearance analysis then the study of  $\nu_e$  CC interactions can provide important additional information on the oscillation mode, since the  $\nu_\mu$  CC energy measurement is largely mode-independent. If two-flavour  $\nu_\mu \rightarrow \nu_e$  oscillations occur, then the values of  $\Delta m^2$  and  $\sin^2 2\theta$  obtained from  $\nu_\mu$  disappearance and  $\nu_e$  appearance fits should be consistent with one another. If two-flavour  $\nu_\mu \rightarrow \nu_\tau$  oscillations occur then no effect will be seen in the  $\nu_e$  appearance analysis<sup>5</sup>. If an oscillation

---

<sup>5</sup> The contribution from  $\tau \rightarrow e$  decays in this analysis is expected to be small and will, in any case, not produce an oscillation signal at the same value of  $\Delta m^2$  and  $\sin^2 2\theta$  as the  $\nu_\mu$  disappearance analysis due to the suppression of the  $\nu_\tau$  CC cross-section and missing energy in the tau decay.

signal is seen in both  $\nu_\mu$  disappearance and  $\nu_e$  appearance analyses then three-flavour mixing, which is discussed in the following chapter, is indicated.